Proceedings of ASME Turbo Expo 2024
Turbomachinery Technical Conference and Exposition
GT2024
June 24-28, 2024, London, United Kingdom

GT2024-127790

BALL BEARING DYNAMIC STIFFNESS PREDICTION CONSIDERING AN UNCERTAIN POSITION OF ROLLING ELEMENTS

Roman Kochurov
SoftInWay, Inc.
Burlington, MA

Volodymyr Martynenko
SoftInWay Switzerland GmbH
Zug, Switzerland

Leonid Moroz
SoftInWay, Inc.
Burlington, MA

Yuriy Govorushchenko
SoftInWay, Inc.
Burlington, MA

ABSTRACT

This paper considers the challenge of calculating accurate ball bearing stiffness, which is attributed to the uncertainty in the rolling element positions; and it solves that issue based on the simultaneous consideration of these positions and the physical effects of the rotating components. The novelty of the paper consists of the suggested methodology to resolve the uncertainty of the rolling element circumferential position when calculating bearing stiffness. The problem is solved through various formulations of dry and lubricated contact and validated based on the consideration of the finite-element model. The algorithms presented in the paper allow for the calculation of the resulting stiffness based on the stiffness values evaluated through different ball bearing positions. The approach presented in the paper is validated based on the experimental data. For this purpose, the model of the rotor in ball bearings is built, along with further calculation of the rotor dynamics. The comparison of the critical speeds calculated for the rotor in bearings, which have stiffness evaluated by the proposed approach with the measurements for the real machine, indicates a high accuracy of the suggested method in comparison with the methods that consider the single position of the rolling element when estimating their stiffness. In the paper, further recommendations for the use of the presented method are given, which will be useful for engineers in the field of turbomachinery dynamics.

Keywords: rolling element; deep groove ball bearing; elasto-hydrodynamic lubrication; stiffness; contact.

1. INTRODUCTION

Rolling element bearings are one of the most popular types of bearings applied to all rotating structures, especially in turbomachinery. They are used much more often in comparison to fluid film bearings considered by Kochurov et al in [1] and active magnetic bearings [2,3], which can apply to very specific cases. They are widely used in both highly loaded applications, like turbojet engines [4–6], and more basic ones, like industrial ventilation – which were discussed by Martynenko in [7].

The use of rolling element bearings in rotating turbomachines raises questions about the correct modeling of the dynamics of rotors installed in rolling element bearings. For this purpose, the stiffness calculation for the rolling element bearing should be accurate when considering it in the rotor dynamics model.

The study of the dynamics of the rolling element bearings, namely the ball ones, started decades ago [8–10]. However, currently, there is no unified approach to the calculation of rolling element bearing stiffness, and each of them has its disadvantages, which were reviewed by Cao et al in [11]. The approaches for the calculation of rolling element bearing stiffness are based on various methods. One of the most popular among those approaches, the Hertz method [12–14], considers a dry contact between the rolling elements and raceways. Another method is elasto-hydrodynamic lubrication (EHL) [15–17], which incorporates lubrication stiffness into the consideration of contact between the rolling elements and raceways. It also encompasses variable formulations of finite-element analysis, transitioning from the static problem of dry contact solved at certain positions of the rolling elements [18,19] to the explicit dynamics problem. This considers the rotation of rolling elements along the circumference of the raceways while the bearing is rotating [20,21].

In most problem formulations, excluding the explicit dynamics formulation, the rolling elements are fixed in the circumferential direction while in their position related to the raceways in order to solve the corresponding contact problem. However, this does not properly consider the real behavior of the rolling element bearing that is connected to the constant rotation of rolling elements along the raceway. Due to this fact, the problem formulations based on the static position of rolling elements either over- or underestimate the rolling element bearing stiffness by not considering all rolling element positions at once. The obvious solution to this obstacle, namely using the explicit dynamics formulation, requires an extremely high amount of computational power. This is caused by the need to

solve the full-bearing finite-element model fine enough to correctly calculate the contact stresses at each moment of time.

As a result, using the existing methods creates uncertainty because of the need to select the rolling element bearing circumferential position before the solution of the problem. However, the problem is well-studied considering the large number of important effects.

One of the promising ways for the analytical investigation into the open questions around the rolling element bearing modeling is the EHL method. It takes both structural and fluid parts of the system into account and has continued to develop in recent years. For example, Bizarre et al in the paper [22] consider the reduced order model for the calculation of the nonlinear stiffness and damping coefficients of the angular contact ball bearing - using the EHL theory to reduce the calculation cost. A similar approach is used by Yan et al [23], but in this paper, the dynamic model of a bearing-housing system is considered. The same principle of application for the EHL method to the calculation of bearing stiffness and damping is also used for modeling line contacts in roller bearings. This is not only in static (see Tsuha and Cavalca [24]) but also in transient formulation, as considered by Fang et al [25].

Further extensions of the EHL ball bearing model are made by using the multi-ellipsoid contact model by Meng et al [26], under multi-factor coupling conditions, taking into account the gyroscopic moment and the axial and radial thermal deformation investigated by Lei et al in [27]. Additionally, the effects of axial preload, as studied by Bal et al. [28], and local defects, as examined by Tian et al. [29] – both previously investigated experimentally [30,31] – are taken into account. The EHL formulation for ball bearings is also capable of considering the time-varying oil film, as shown by Xu et al in [32]. Separate attention should be given to the fact that the EHL theory for rolling element bearings is also capable of considering both oil and grease as lubricants, which was experimentally proven by recent works [33–35].

The current paper uses the EHL methodology to calculate the speed- and load-dependent stiffness properties of the deep groove ball bearings (DGBB), which are the supports of the industrial fan rotor. To focus on the effects influencing the bearing response under the changing radial load and rotational speed, the approach suggests determining the unified radial stiffness (which is sufficient information for most lateral rotor dynamics models) in contrast to the classical 5-DOF model, which provides more information regarding the bearing degrees of freedom. However, they give a more complex output, which increases the requirements for the rotor modeling and is not necessary for the goals of this study. Some grease effects occurring in the rolling element bearings (thickener, starvation) got out of the scope of the study based on the experimental studies mentioned above, which were discussed in the literature research. The novelty of the technique exists when considering the multiple rolling element positions in the bearing circumference, and taking into account the variable number of active rolling elements depending on the applied load.

2. PROBLEM FORMULATION

The current section presents a brief description of the EHL theory for ball bearings, a discussion of the case used for the calculation of the results, and some key features of the considered design of the fan.

2.1 Theoretical Background

As the modern finite-element codes allow the simulation of highly nonlinear complex designs [36], the finite-element approach was used for modeling the rotor dynamics response.

The rotor dynamics transient response is simulated based on a full system of dynamic equations of the elasticity theory. This includes a Timoshenko beam assumption discretized by the finite element method in the fixed coordinate system [37]:

$$[M]\{\ddot{w}(t)\} + ([C] + \Omega[G])\{\dot{w}(t)\} + [K]\{w(t)\} = \{F_{ext}\}, \quad (1)$$

where $\{w(t)\}^T = \{X(t), Y(t)\}^T$ is the nodal displacement vector; $[M]$, $[C]$, $[G]$, $[K]$ are global mass, damping (including bearing damping), gyroscopic, and stiffness (including bearing stiffness) matrices; $\{F_{ext}\}^T$ is the external force vector; Ω is the rotor rotational speed.

For the determination of the undamped critical speeds, the full equation (1) is simplified, and the following eigenvalue problem is solved:

$$([K] - \omega_i^2[M(\gamma)])\{w_i\} = 0, \quad (2)$$

where ω_i $(i = 1,2, \dots, N)$ are the natural frequencies (critical speeds) of the system; $\{w_i\}$ are the mode shapes; $[M(\gamma)]$ is the matrix which includes all inertia effects (mass and Coriolis); γ is the spin whirl ratio, which indicates the type of rotor whirl (1 is the forward whirl, -1 is the backward whirl, etc.).

In the case of the harmonic loading due to unbalance $\{F_{ext}\} = \{F_c\}\cos(\Omega t) + \{F_s\}\sin(\Omega t)$, the steady state response of the system $\{w_{ext}\} = \{w_c\}\cos(\Omega t) + \{w_s\}\sin(\Omega t)$ is determined by the following simplification of the equation (1):

$$\begin{bmatrix} [K] - \Omega^2[M] & \Omega([C] + \Omega[G]) \\ -\Omega([C] + \Omega[G]) & [K] - \Omega^2[M] \end{bmatrix} \begin{Bmatrix} \{w_c\} \\ \{w_s\} \end{Bmatrix} = \begin{Bmatrix} \{F_c\} \\ \{F_s\} \end{Bmatrix}. \quad (3)$$

As mentioned above, the matrix $[K]$ contains not only terms associated with the finite-element discretization of the rotor but also bearing stiffness values in the corresponding rotor nodes, which are calculated by the EHL methodology based on the combination of the Hertz solution and EHL correction.

According to the Hertz solution, the area of contact of two bodies with curvature radii R_{x1}, $R_{y1,}$ and R_{x2}, R_{y2} is represented by the ellipse with the axes *a* and *b* with the deformation *c* under the applied load *f*. These parameters are described by the formulas:

$$\begin{gathered} a = \left(\frac{6R\kappa\mathcal{E}}{E'\pi}\right)^{1/3} f^{1/3} \\ \kappa = \frac{a}{b} < 1 \\ c = \frac{\mathcal{K}\kappa^{2/3}}{\mathcal{E}^{1/3}}\left(\frac{3}{\sqrt{2R}E'\pi}\right)^{2/3} f^{2/3} \end{gathered} \Rightarrow, \quad (4)$$

where $R = 1/(1/R_x+1/R_y)$ is the full reduced radius; $R_x = 1/(1/R_{x1}+1/R_{x2})$ is the reduced radius of two bodies in x direction; $R_y = 1/(1/R_{y1}+1/R_{y2})$ is the reduced radius of two bodies in y direction; E' is the reduced elasticity modulus; κ is the ellipticity parameter which is the solution of the algebraic equation:

$$\frac{R_x}{R_y} = \kappa^2 \frac{\mathcal{K}-\mathcal{E}}{\mathcal{E}-\kappa^2\mathcal{K}}, \quad (5)$$

where $\mathcal{K} = \mathcal{K}(1-\kappa^2)$ and $\mathcal{E} = \mathcal{E}(1-\kappa^2)$ are the elliptical integral of the first and second kind:

$$\begin{gathered} \mathcal{K}(1-\kappa^2) = \int_0^{\pi/2}(1-(1-\kappa^2)^2\sin^2\phi)^{-1/2}d\phi \\ \mathcal{E}(1-\kappa^2) = \int_0^{\pi/2}(1-(1-\kappa^2)^2\sin^2\phi)^{1/2}d\phi \end{gathered}. \quad (6)$$

The stiffness coefficient of two deformed contacting bodies is determined by differentiation of the force f by the contact deformation c:

$$k = \frac{df}{dc} = \frac{\pi}{2}\frac{\mathcal{E}^{1/2}}{\mathcal{K}^{3/2}\kappa}E'\sqrt{2R}c^{1/2}. \quad (7)$$

Keeping in mind that there are two sets of contacting bodies for the rolling element bearing, the inner ring-ball and ball-outer ring, and neglecting the influence of centrifugal and gyroscopic effects on the force balance in the rolling element bearing, the contact deformation for the inner and outer sets c_i and c_o are calculated with respect to their own parameters by the previous formulas. The forces on the inner and outer set f_i and f_o are equal $f_i = f_o = f$, the total deformation $\delta = c_i + c_o$, and the stiffness of a single ball contacting inner and outer raceways is calculated by the formula $k = \frac{df}{d\delta}$.

Assembling the contacting bodies into a whole bearing that has Z rolling elements, and considering the presence of the radial clearance C_r between the balls and raceways, the following static equilibrium equation can be used:

$$F_r = \sum_{\Psi=0}^{\Psi=\pm i\Delta\Psi} F_\Psi \cos\Psi, \Delta\Psi = \frac{2\pi}{Z}, \quad (8)$$

where $F_\Psi = F_\Psi(\delta_\Psi)$ is the force calculated by the previously described rules for the deformation of the arbitrary ball located at the angle Ψ to the vertical axis [12]:

$$\delta_\Psi = \delta_r \cos\Psi - \frac{1}{2}C_r, \quad (9)$$

where δ_r is the displacement of the shaft.

On top of that, the EHL correction $\Delta(N, L)$ [16] is added to the deformation of the dry contact c shown in (4) to get the full lubricated contact deformation $\delta = \Delta(N, L)c$:

$$\begin{gathered} \Delta(N,L) = 1 - p(L)N^{q(L)} \\ N = \sqrt{\frac{R_x}{R_y}}M \\ p(L) = ((4-0.2L)^7 + (3.5+0.1L)^7)^{1/7} \\ q(L) = -\left(0.6 + 0.6(L+3)^{-1/2}\right) \end{gathered}, \quad (10)$$

where L and M are the non-dimensional Moes parameters describing the bearing's physical and geometrical parameters, along with the contacting element reference velocity dependent on the bearing rotational speed [38]. This dependence on the rotational speed results in its influence on the bearing stiffness calculated by the EHL method.

Equation (10) neglects some additional effects that are inherent with high speeds and changing the film thickness. Therefore, the bearing is assumed to rotate at relatively low speeds. After finishing the calculation based on the equations shown above, that allows for the calculation of a bearing stiffness. However, that depends on a rolling element position along the circumference, which in turn creates uncertainty in the results. To avoid this uncertainty, the energy balance equation is used to select the exact value of stiffness for certain values of the radial load and rotational speed, considering two border cases of a single ball located in the bottom of the bearing (the load acting 'on the ball') and two balls symmetrically located in the bottom of the bearing (the load acting 'between balls') which is illustrated in the practical example shown in the further sections. This approach gives a more accurate value of the bearing stiffness when considering different numbers of active balls for the variable load and speed.

2.2 Rotor and Bearing Models

The paper [7] considered a rotor of the axial industrial fan to determine its static strength and modal characteristics based on the three-dimensional finite element approach, which allows for the calculation of the mode shapes associated with the vibrations of the blades, the disc, the shaft, etc. However, in this paper, only the first six natural frequencies were considered, which were not associated with the shaft deflection, and the bearings were modeled as rigid since the rotor dynamics natural frequencies were higher than the considered natural frequencies.

The current paper suggests considering this rotor shown in the scheme in Figure 1 to discretize it with the Timoshenko beam finite elements, which is shown in Figure 2 for the accurate consideration of the rotor dynamics response. This takes the effects of shaft rotation and bearing compliance into account.

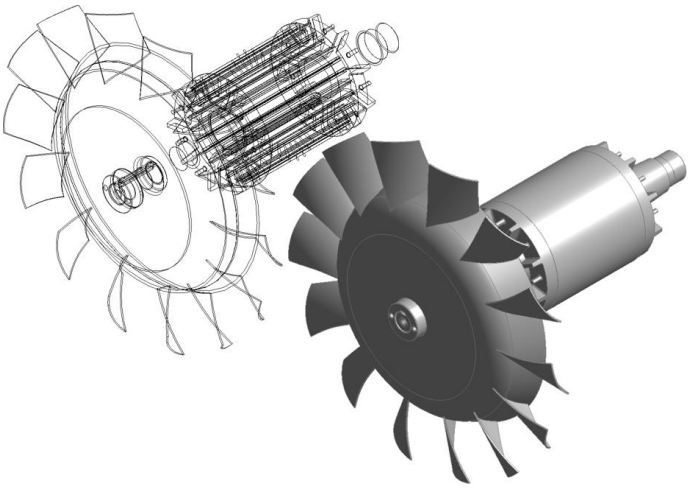

FIGURE 1: THE SCHEMATIC AND SOLID VIEWS OF THE THREE-DIMENSIONAL MODEL OF THE AXIAL FAN

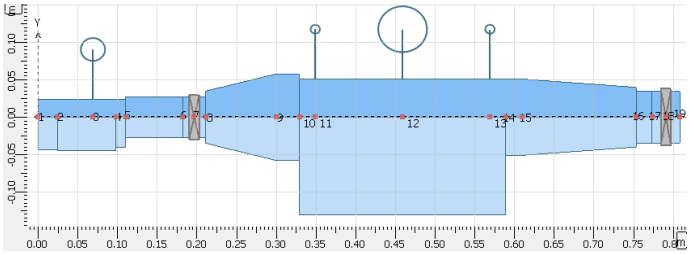

FIGURE 2: THE AXIAL FAN ROTOR DYNAMICS MODEL

In Figure 2, the blue color indicates the mass diameters of the sections (i.e. the diameters of equivalent axisymmetric shaft sections which have the same mass as the actual shaft ones), the light blue color shows the stiffness diameters of the sections (i.e. the diameters of equivalent axisymmetric shaft sections which have the same lateral stiffness as the actual shaft ones), the circles represent the mass-inertia elements with a certain mass and mass moments of inertia (from left to right – the impeller, the first part of the aluminum motor core, the steel motor part, the second part of the aluminum motor core), and the grey rectangles show the bearing locations (the left one is the front bearing and the right one is the rear bearing).

The majority of attention is focused on accurately calculating the bearing stiffness coefficients based on the EHL approach described above while considering the uncertainties discussed in the introduction section and those associated with the changing position of the rolling elements during rotor rotation.

The bearings used in the considered rotor are deep groove ball bearings with the designations SKF 6311-2Z C3 and SKF 6014-2Z C3 for the front and rear bearings respectively. The bearings have increased radial clearance to prevent heating issues, which may result in additional challenges in the calculation of their stiffness coefficients. Experimentally, there was validation that the transition from the normal bearing clearance to the increased ones fixes the issues associated with the heating effects, therefore the current approach leaves them out of the scope of its study.

The scheme of the bearings is shown in Figure 3 and the bearing geometrical, physical, and operational parameters used in the calculation are shown in Table 1.

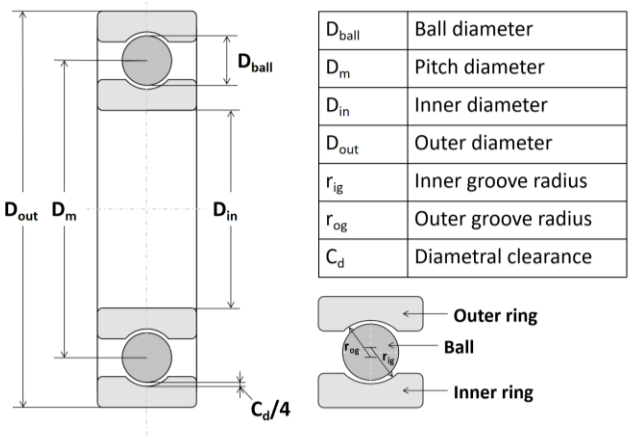

D_{ball}	Ball diameter
D_m	Pitch diameter
D_{in}	Inner diameter
D_{out}	Outer diameter
r_{ig}	Inner groove radius
r_{og}	Outer groove radius
C_d	Diametral clearance

FIGURE 3: DEEP GROOVE BEARING SCHEME

TABLE 1: BEARING PARAMETERS

Input	Bearing	
	Front	Rear
Designation by SKF	6311-2Z C3	6014-2Z C3
Ball diameter [mm]	20.638	11.906
Number of balls [-]	8	14
Diametral clearance [mm]	0.033	0.038
Bearing pitch radius [mm]	43.75	45
Inner groove radius [mm]	10.73176	6.19112
Outer groove radius [mm]	10.93814	6.31018
Ball elastic modulus [Pa]	2.1e11	2.1e11
Ball Poisson ratio [-]	0.3	0.3
Ring Young moduli [Pa]	2.1e11	2.1e11
Ring Poisson ratios [-]	0.3	0.3
Temperature [C]	60	60
Press. viscosity coef. [Pa^{-1}]	2.35909e-08	2.35909e-08
Viscosity [Pa s]	0.063	0.063
Contact type [-]	Ellipse	Ellipse
Radial load [N]	1098.976	480.8368
Rotational speed [rpm]	3000	3000
Loss factor [-]	0.02	0.02

The middle of the manufacturing tolerance range was used for calculations of both SKF 6311-2Z C3 and SKF 6014-2Z C3 bearings. The inner and outer groove radii r_i and r_e were calculated based on the ball diameter D_w according to the ISO 16281 standard by the following formulas: $r_i = 0.52*D_w$; $r_e = 0.53*D_w$.

2.3 Features of the Design

The loads on the bearings shown in Table 1 were calculated based on the static analysis of the Timoshenko beam finite-element model under the gravity load. Figure 4 shows the deflection form of the rotor in these conditions having the maximal displacement at the impeller end equal to 5.76 µm.

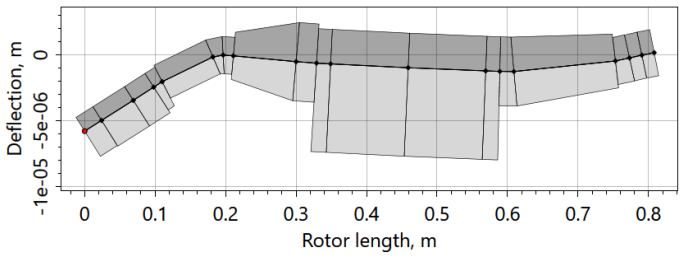

FIGURE 4: ROTOR DEFLECTION FORM UNDER THE GRAVITY LOAD

For the rigid bearing assumption (the stiffness of the bearings is two orders of magnitude higher than the stiffness of the rotor), the loads on the bearings were calculated because the real bearing stiffness is unknown at this stage of analysis.

It is also valuable to calculate the modal properties of the rotor in rigid bearings in order to determine the possible sources of resonances before the analyses in flexible bearings. Figure 5 shows the undamped Campbell diagram with the first backward whirl mode shape at the critical speed of 4899 rpm, and the first forward whirl mode shape at the critical speed of 25259 rpm.

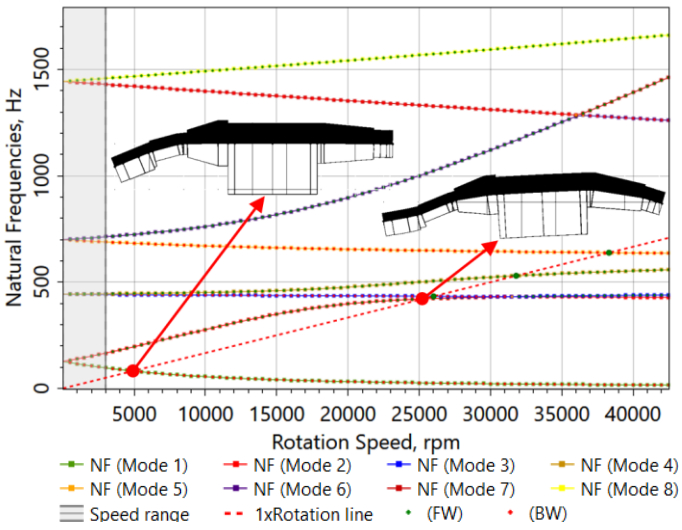

FIGURE 5: UNDAMPED CAMPBELL DIAGRAM OF THE ROTOR IN RIGID BEARINGS

The rotor rotational speed range up to 3000 rpm is shown in grey in the figure. As it follows from this figure, the margin from the operational speed to the first backward whirl critical speed is about 60%, which is acceptable. However, with flexible bearings, the corresponding critical speeds can get lower and closer to the rotor rotational speed. This is even more obvious for the forward whirl critical speed, which for the bearing stiffness 1e7 N/m, reaches the exact value of the operational speed as can be seen in the critical speed map in Figure 6.

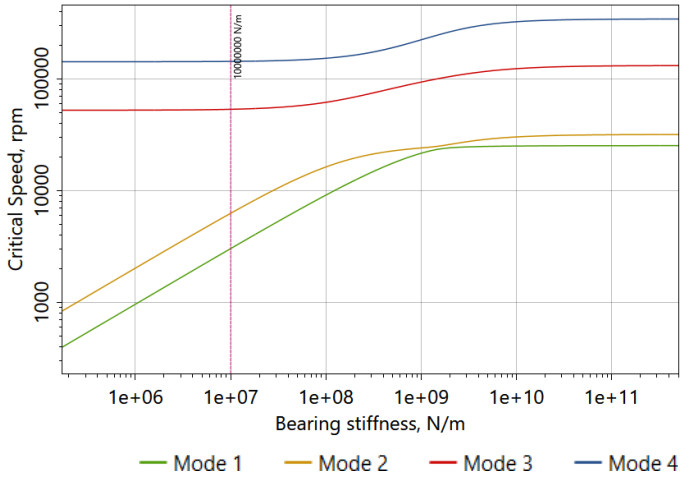

FIGURE 6: FORWARD WHIRL CRITICAL SPEED MAP

Therefore, it is highly important to calculate the stiffness of the bearings accurately because it is crucial when correctly determining the margin between the operational speed and the real rotor critical speeds.

3. RESULTS AND DISCUSSION

The current section presents the results of the study which were verified using the finite-element model of the bearing.

3.1 Verification of the DGBB Stiffness Calculation

The calculation of the deep groove ball bearing stiffness was verified by the static finite-element (FE) analysis performed for cases with load acting 'on the ball' and 'between balls' – see Figure 7.

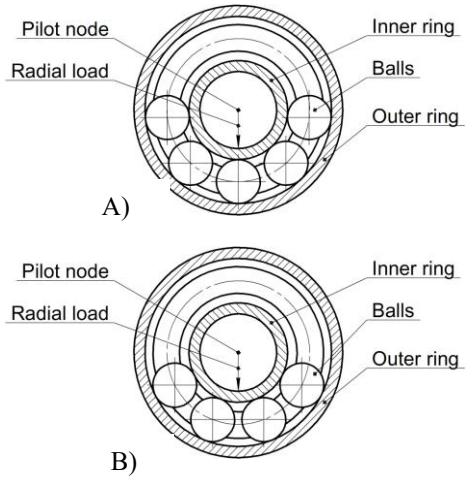

FIGURE 7: CONSIDERED CASES: A) LOAD ACTING 'ON THE BALL'; B) LOAD 'BETWEEN BALLS'

Finite-element models were built for both cases – with one and two balls in the bottom of the bearing both with and without the radial clearance.

The finite-element (FE) model for the case with the load on the ball (one ball in the bottom) case is shown in Figure 8 for SKF 6311-2Z C3 bearing.

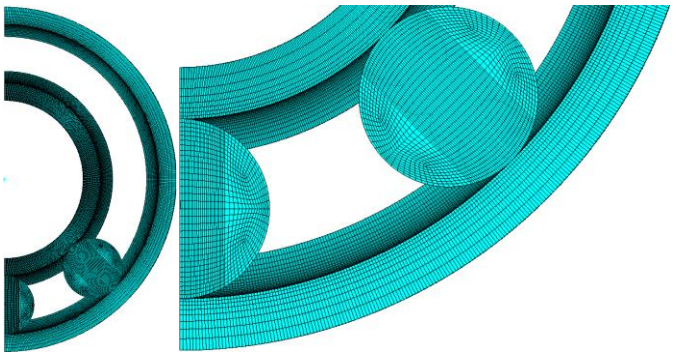

FIGURE 8: DGGB FE MESH (LOAD ON THE BALL CASE)

The displacements of the outer surface of the outer ring were fixed in all directions. The symmetry conditions were used, and all the balls in the top half of the bearing were removed to reduce the problem size. The rigid connection of the remote point in the center of the bearing to the inner surface of the ring was established, and the load was applied to this remote point. The nonlinear contacts were specified for the inner raceway-ball and ball-outer raceway surfaces. The discretization error was ensured to be within the 2% engineering accuracy before the calculations (i.e. a grid refinement study has been performed to make sure that the discretization error is smaller than 2%). Variable loads were considered for all calculated cases and load directions.

To calculate the stiffness of the bearing, two loads $F_{r\,1}$ and $F_{r\,1.01}$ were applied. They correspond to the values of 100% and 101% load, which the stiffness is calculated based off of respectively. The values of the remote point displacements δ_1 and $\delta_{1.01}$ were calculated in the finite-element code, and the bearing stiffness was determined by the relation $k(F_r) = (F_{r\,1.01} - F_{r\,1})/(\delta_{1.01} - \delta_1)$.

The lubrication was not considered in the finite-element model, therefore it modeled the dry contact conditions. For comparison purposes, since the finite-element calculation cannot take the presence of the fluid film into account, the zero lubricant viscosity was set in the EHL calculations.

Figure 9 shows the comparison between the stiffness calculated for different loads up to the workload by the finite-element method (FEM) and the EHL method with zero viscosity and zero clearance.

As it follows from Figure 9, the developed method shows sufficient accuracy in comparison with the FEM. For the zero clearance cases, there are no steps in the stiffness-load curves.

Substantially different effects were obtained for the cases with non-zero clearances. In this case, the bearing preload due to the applied radial load results in a different number of active balls (balls in contact) depending on the values of this load (the higher the load is, the more balls are in contact which is properly modeled by the EHL code). Figure 10 shows results obtained by FEM for the cases with loads ‘on’ and ‘between’ balls. This simulation doesn’t include the lubrication effect.

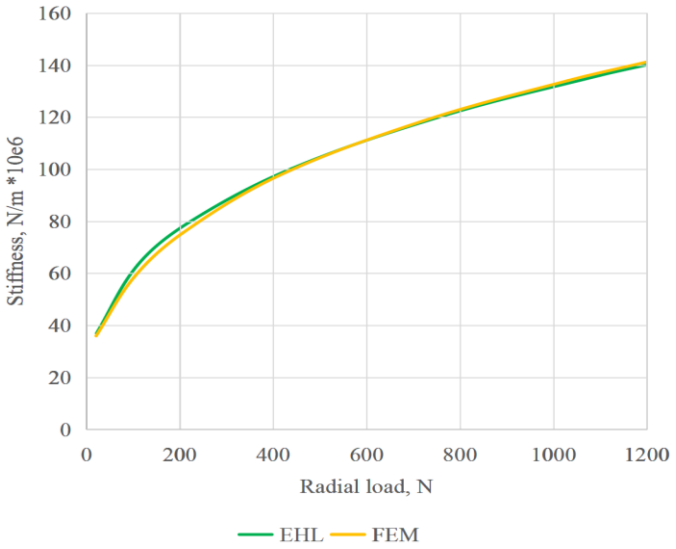

FIGURE 9: VERIFICATION PLOT FOR THE EHL METHOD BY THE FEM FOR THE ZERO CLEARANCE CASE

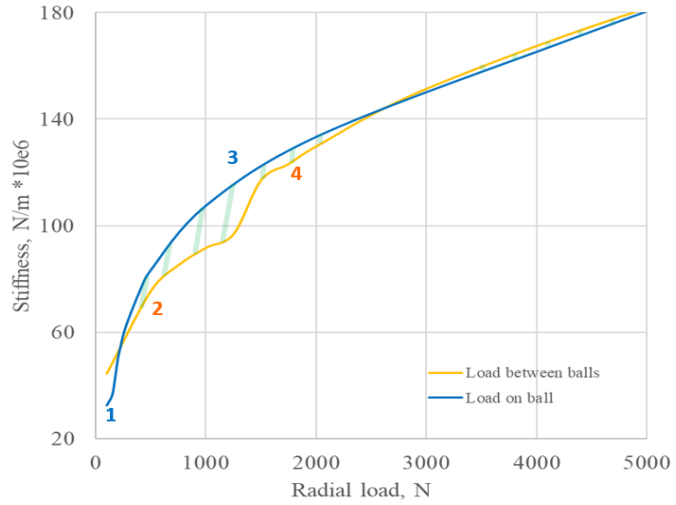

FIGURE 10: PLOT CALCULATED BY THE FEM FOR THE NON-ZERO CLEARANCE CASE

Separately, the finite-element method considers load ‘on’ a ball and ‘between’ balls: the blue line corresponds to the case of load ‘on the ball’ and the yellow line corresponds to the case of loading ‘between’ balls. It could be observed several bends at load around 200 N for the ‘load on ball’ case and at 1300 N for the ‘between ball’ load case. This is a result of active balls numbers changing from 1 to 3 and from 2 to 4 correspondingly. For the real physical system, the stiffness will be different and most of all, inside the marked areas as balls are rotating with the

cage speed. Thus, the deviation in stiffness coefficients reaches 11% and will lead to an unacceptable discrepancy in critical speed analysis results for the rotor-bearing system.

3.2 Stiffness Calculation of DGBB with Lubrication

The developed algorithm allows the determination of the bearing stiffness, considering the changed position of the balls and the number of active balls vs. load based on the principle of minimum potential energy. As a result, the simultaneous consideration of the one ball in the bottom and two balls in the bottom cases is the benefit of the created method for the calculation of the deep groove ball bearing stiffness.

Figure 11 and Figure 12 represent the stiffness calculation of SKF 6311-2Z C3 and SKF 6014-2Z C3 bearing with the geometrical and physical parameters in Table 1 calculated for the range of rotational speeds from 0 to 6500 rpm in the case of lubricated contact with corresponding clearances.

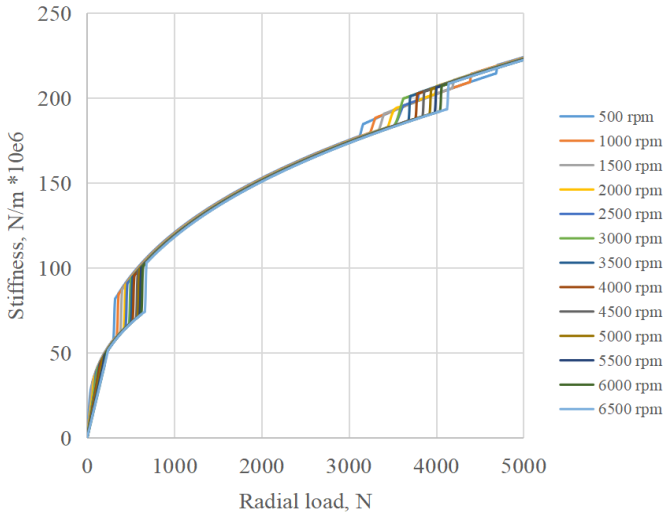

FIGURE 11: STIFFNESS VS LOAD PLOT FOR SKF 6311-2Z C3

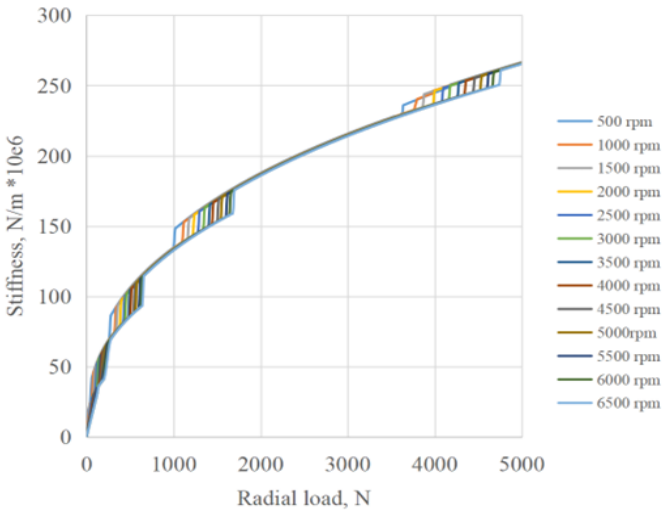

FIGURE 12: STIFFNESS VS LOAD PLOT FOR SKF 6014-2Z C3

Note that Figure 10 and Figure 11 cannot be compared directly because the first one considers the dry conditions comparable with the Hertz solution (a zero viscosity case for the EHL formulation), while the second one presents the results of the lubricated contact consideration. This takes into account the effect of lubrication on the contact stiffness of the solid deformable bodies, incorporating the lubricant stiffness itself and evaluating the impact of the active ball number on the bearing response. That causes the obvious jumps on the stiffness vs radial load plots.

As seen in these figures, for SKF 6311-2Z C3, which has 8 balls, there are four shifts in the stiffness-load curve, which correspond to the gradual increase of load and stepped increase of active balls in the contact (in the first step, a single ball is in contact, then, with increased load, two balls starts contacting instead of one and so on up to four balls available in the bottom half of the bearing). For SKF 6014-2Z C3, there are six steps in the plot because the maximum of six balls can be located in the bottom half of the bearing.

This indicates that the proposed technique allows for the consideration of uncertain rolling element bearing position and the determination of 'active' balls for the variable load.

Figure 13 and Figure 14 show the pressure and fluid film thickness distributions for the most loaded rolling element of SKF 6311-2Z C3 bearing at the operating load of 1099 N (see Table 1). The top pictures in each figure correspond to the contact between the inner raceway and the ball. The bottom pictures in each figure correspond to the contact between the ball and the outer raceway. The value of stiffness for this bearing under the operating load and speed of 3000 rpm is 123.2 MN/m.

Figure 15 and Figure 16 show the pressure and fluid film thickness distributions for the most loaded rolling element of SKF 6014-2Z C3 bearing at the operating load of 480.8 N (see Table 1). The top pictures in each figure correspond to the contact between the inner raceway and the ball, and the bottom pictures in each figure correspond to the contact between the ball and the outer raceway. The value of stiffness for this bearing under the operating load at the operating speed of 3000 rpm is 103.02 MN/m.

The horizontal axis in the figures shows the rolling direction, the axis perpendicular to the direction of view is the transverse direction, and the vertical axis is the dimensionless value of the investigated parameters, which were calculated for pressure and film thickness by dividing the dimensional ones by the maximal Hertzian pressure p_h and deformation c respectively.

Note that for the dimensionless film thickness plots, the value $2 - H$ (where H is the actual dimensionless film thickness) is shown on the vertical axis to improve the representation of the plot. That explains zones of negative values as well as zones where the $2 - H$ parameter exceeds the value 2 (in these zones elastic deformations of contacting rolling elements and raceways occur). In addition, Figure 13 shows one vs two pressure 'spikes' for inner ring-ball and ball-outer ring contacts, which can be explained by the difference in raceway curvatures in the circumferential direction (positive curvature of the inner ring raceway vs negative curvature of the outer ring raceway).

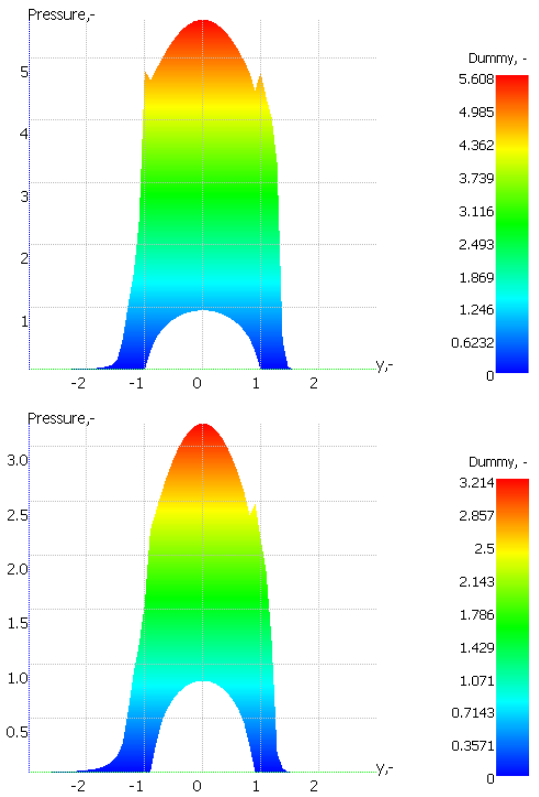

FIGURE 13: FLUID FILM PRESSURE FOR SKF 6311-2Z C3

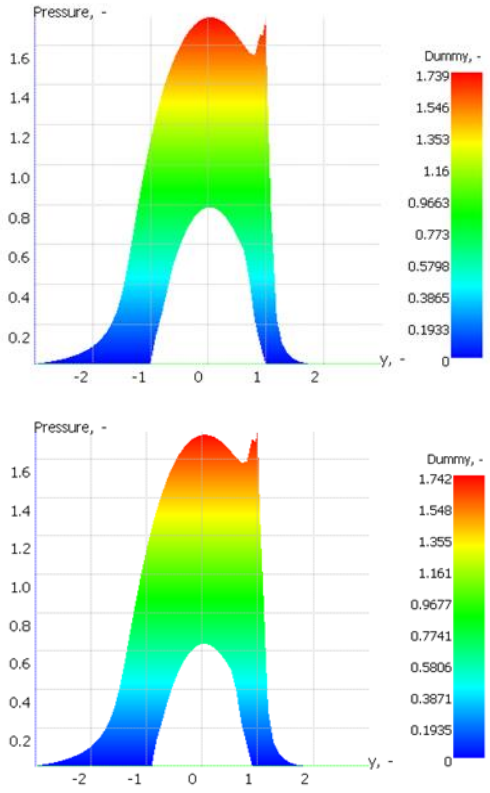

FIGURE 15: FLUID FILM PRESSURE FOR SKF 6014-2Z C3

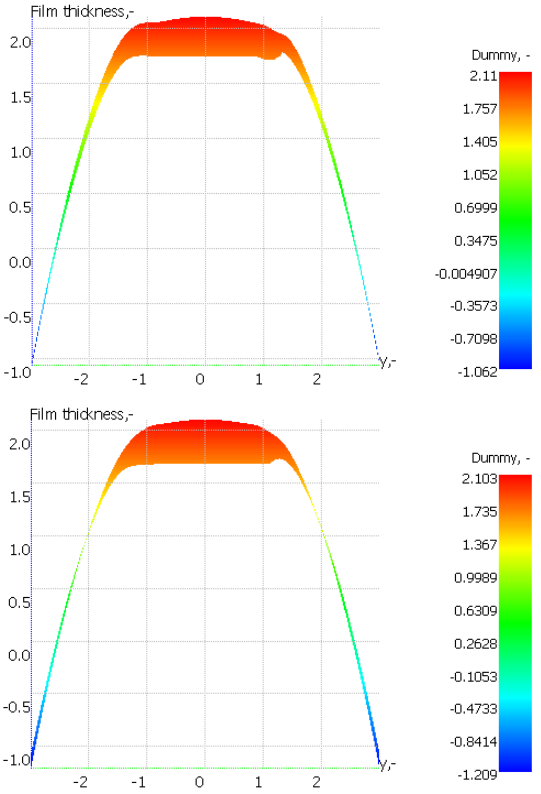

FIGURE 14: FLUID FILM THICKNESS FOR SKF 6311-2Z C3

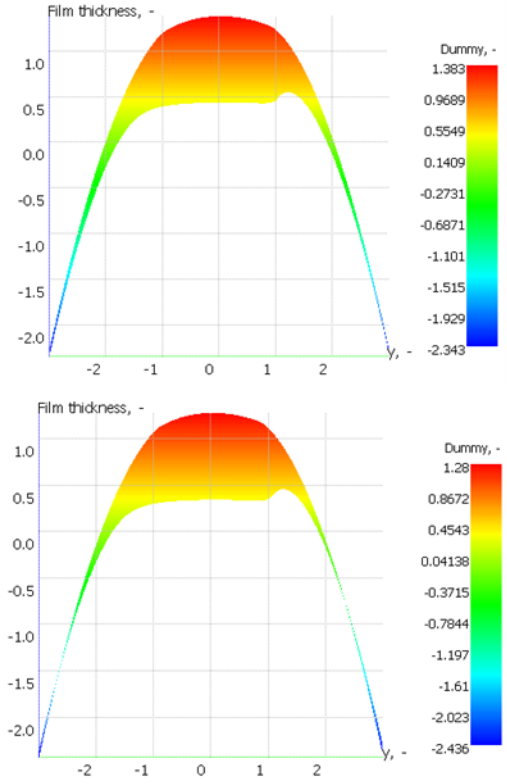

FIGURE 16: FLUID FILM THICKNESS FOR SKF 6014-2Z C3

Additionally, the dependence of the bearing stiffness on the rotational speed was calculated and considered accordingly.

Therefore, the stiffness values of both bearings, taking into account the increased gap, presence of lubrication, and uncertainty of the rolling element bearing position, were determined. They are ready to be used in the calculation of the dynamics of the rotor in flexible bearings.

It should be noted that most of publications at the current state of problem development consider the significant impact of axial preload on the bearing radial stiffness only in cases of angular contact ball bearings with non-zero contact angles [28, 39–41] while the current paper develops an approach for the deep groove bearing which is an equivalent of angular contact ball bearings with zero contact angle. In addition, the aerodynamic thrust for the axial fan is small in comparison to other turbomachines, while significant artificial preloads are not applied for this design due to maintenance reasons. These factors allowed bringing the axial preload consideration out of scope of this study.

3.3 Rotor Dynamics with the Calculated Stiffness

Figure 17 presents the undamped Campbell diagram for the case of flexible bearings, with the stiffness calculated using the developed method. The first undamped backward and forward whirl critical speeds have values of 4706 rpm and 9803 rpm, and the corresponding mode shapes are shown in Figure 18 and Figure 19.

According to these results, considering the flexible bearings with stiffness calculated by the developed method leads to a 158% drop in the first forward whirl critical speed (compared to the rigid bearings case), potentially significantly impacting the rotor's resonant state, especially at operational speeds higher than 3000 rpm. The change in the first backward whirl critical speed is less significant, at around 5%.

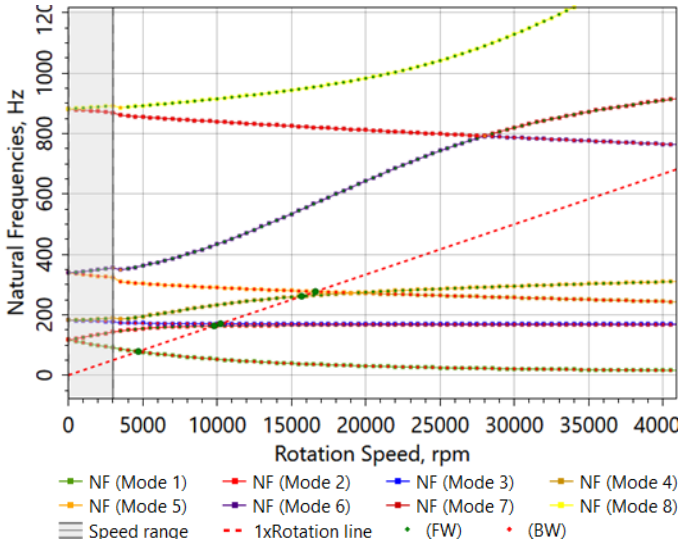

FIGURE 17: CAMPBELL DIAGRAM OF THE ROTOR IN FLEXIBLE BEARINGS

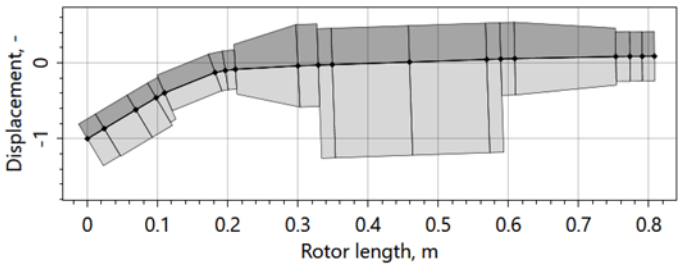

FIGURE 18: FIRST UNDAMPED BACKWARD WHIRL MODE SHAPE CORRESPONDING TO THE CRITICAL SPEED 4706 RPM

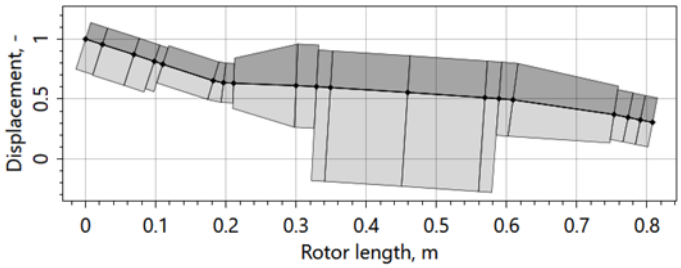

FIGURE 19: FIRST UNDAMPED FORWARD WHIRL MODE SHAPE CORRESPONDING TO THE CRITICAL SPEED 9803 RPM

Additional simulations were performed with bearing stiffnesses calculated by FEM, where the minimum and maximum stiffness values were considered, (results for different numbers of active balls) and lubrication influence was excluded. For the minimal stiffness, the rotor critical speed is 4648 rpm and 8730 rpm. For the maximal stiffness, the corresponding critical speeds are 4701 rpm and 9673 rpm. Thus, the uncertainty of the rotor critical speed calculation due to the uncertain number of active balls is up to 11% at operating load, which can be critical for rotordynamics acceptance conclusions.

4. CONCLUSIONS

The paper presents the EHL approach for the determination of the speed-dependent bearing stiffness, which takes into account the non-zero bearing clearance, lubrication properties, and uncertain rolling element position. The methodology is verified using FEM and used for the rotor dynamics calculation of the axial fan rotor. The deviation of the rotor critical speeds as the result of the uncertainty of ball position has been studied and this difference reaches up to 11%. The practical result of the developed method is that it allows for more accurate results for the ball bearing stiffness, and consequently more accurate rotor critical speeds.

REFERENCES

[1] Kochurov, R., Moroz, L., and Martynenko, V., 2023, "Nonlinear Response of the Rotor Supported by Gas Journal Bearings Considering Stationary and Rotating Herringbone Grooves," *Proceedings of the ASME Turbo Expo 2023: Turbomachinery Technical Conference and Exposition. Volume 11B*, American Society of Mechanical Engineers, Boston, Massachusetts, USA, pp. 1–12.

[2] Martynenko, G., and Martynenko, V., 2021, "Computer Modeling and Simulation Analysis of Linear and Nonlinear Phenomena of Rotor Dynamics in Systems with Magnetic Bearings," *2021 IEEE 2nd KhPI Week on Advanced Technology (KhPIWeek)*, IEEE, pp. 213–217.

[3] Martynenko, G., and Martynenko, V., 2021, "Identification of Computational Models of the Dynamics of Gas Turbine Unit Rotors with Magnetic Bearings by Incomplete Data for Design Automation," *Lecture Notes in Networks and Systems*, pp. 451–463.

[4] Merculov, V., Kostin, M., Martynenko, G., Smetankina, N., and Martynenko, V., 2022, "Force Simulation of Bird Strike Issues of Aircraft Turbojet Engine Fan Blades," *Lecture Notes in Networks and Systems*, pp. 129–141.

[5] Merculov, V., Kostin, M., Martynenko, G., Smetankina, N., and Martynenko, V., 2022, "Improving the Accuracy of the Behaviour Simulation of the Material of the Turbojet Aircraft Engine Fan Rotor Blades in the Event of a Bird Strike by Using Adapted Finite Element Computational Models," Mater Today Proc, **59**, pp. 1797–1803.

[6] Merculov, V., Kostin, M., Martynenko, G., Smetankina, N., and Martynenko, V., 2022, "Peculiarities of the Modelling of the Bird Dynamic Impact on Fan Blades of an Aircraft Turbojet Engine at Operating Modes," *Lecture Notes in Networks and Systems*, pp. 462–473.

[7] Martynenko, V., 2020, "Analysis of Strength and Bearing Capacity of the Auxiliary Mine Ventilation Fan Connected to the Rotor of Its Electrical Drive," *2020 IEEE KhPI Week on Advanced Technology (KhPIWeek)*, IEEE, pp. 19–23.

[8] Gupta, P. K., 1979, "Dynamics of Rolling-Element Bearings Part III: Ball Bearing Analysis," Journal of Lubrication Technology, **101**(3), pp. 312–318.

[9] Gupta, P. K., 1979, "Dynamics of Rolling-Element Bearings Part IV: Ball Bearing Results," Journal of Lubrication Technology, **101**(3), pp. 319–326.

[10] Houpert, L., 1997, "A Uniform Analytical Approach for Ball and Roller Bearings Calculations," J Tribol, **119**(4), pp. 851–858.

[11] Cao, H., Niu, L., Xi, S., and Chen, X., 2018, "Mechanical Model Development of Rolling Bearing-Rotor Systems: A Review," Mech Syst Signal Process, **102**, pp. 37–58.

[12] Harris, T. A., and Kotzalas, M. N., 2006, *Rolling Bearing Analysis - 2 Volume Set*, CRC Press.

[13] Houpert, L., 2014, "An Enhanced Study of the Load-Displacement Relationships for Rolling Element Bearings," J Tribol, **136**(1).

[14] Houpert, L., 2015, "Load-Displacement Relationships for Ball and Spherical Roller Bearings," J Tribol, **137**(2).

[15] Wensing, J. A., 1998, "On the Dynamics of Ball Bearings," University of Twente.

[16] Wijnant, Y. H., 1998, "Contact Dynamics in the Field of Elastohydrodynamic Lubrication," University of Twente.

[17] Greenwood, J. A., 2020, "Elastohydrodynamic Lubrication," Lubricants, **8**(5).

[18] Guo, Y., and Parker, R. G., 2012, "Stiffness Matrix Calculation of Rolling Element Bearings Using a Finite Element/Contact Mechanics Model," Mech Mach Theory, **51**, pp. 32–45.

[19] Zhao, H., Wu, W., Li, X., and Li, H., 2013, "Stiffness Analysis of Angular Contact Ball Bearing under Non-Uniform Preload," *Proceedings - 2013 IEEE International Symposium on Assembly and Manufacturing, ISAM 2013*, pp. 97–101.

[20] Singh, S., Köpke, U. G., Howard, C. Q., and Petersen, D., 2014, "Analyses of Contact Forces and Vibration Response for a Defective Rolling Element Bearing Using an Explicit Dynamics Finite Element Model," J Sound Vib, **333**(21), pp. 5356–5377.

[21] Luo, H., Fu, J., Yu, C., Liu, G., Wang, W., and Wang, P., 2018, "Numerical Simulation and Experimental Testing of Dynamic Stiffness of Angular Contact Ball Bearing," Advances in Mechanical Engineering, **10**(9), p. 168781401879897.

[22] Bizarre, L., Nonato, F., and Cavalca, K. L., 2018, "Formulation of Five Degrees of Freedom Ball Bearing Model Accounting for the Nonlinear Stiffness and Damping of Elastohydrodynamic Point Contacts," Mech Mach Theory, **124**, pp. 179–196.

[23] Yan, P., Yan, C., Wang, K., Wang, F., and Wu, L., 2020, "5-DOF Dynamic Modeling of Rolling Bearing with Local Defect Considering Comprehensive Stiffness under Isothermal Elastohydrodynamic Lubrication," Shock and Vibration, **2020**.

[24] Tsuha, N. A. H., and Cavalca, K. L., 2020, "Stiffness and Damping of Elastohydrodynamic Line Contact Applied to Cylindrical Roller Bearing Dynamic Model," J Sound Vib, **481**.

[25] Fang, C., Zhu, A., Zhou, W., Peng, Y., and Meng, X., 2022, "On the Stiffness and Damping Characteristics of Line Contacts under Transient Elastohydrodynamic Lubrication," Lubricants, **10**(4).

[26] Meng, F., Zheng, Y., Liu, Y., Gong, J., and Wang, B., 2020, "Multi-Ellipsoid Contact Elastohydrodynamic Lubrication Performance for Deep Groove Ball Bearing," Tribol Int, **150**.

[27] Lei, C., Cui, P., Cao, P., Liu, K., and Song, R., 2021, "Research on Comprehensive Stiffness Characteristics of Angular Contact Ball Bearings under Multi-Factor Coupling Condition," Journal of Advanced Mechanical Design, Systems and Manufacturing, **15**(6).

[28] Bal, H., Ateş, K., Karaçay, T., and Aktürk, N., 2022, "Effect of Preload on the Vibrations of EHL Angular Contact Ball Bearings: Theoretical and Experimental Results," Lubricants, **10**(3).

[29] Tian, Y., Yan, C., Liu, Y., Kang, J., Lu, Z., and Wu, L., 2023, "Dynamic Modelling of Deep Groove Ball Bearings with Different Local Defects Considering Skidding and Thermal Elastohydrodynamic

Lubrication," Proceedings of the Institution of Mechanical Engineers, Part K: Journal of Multi-body Dynamics, **237**(3), pp. 511–533.
[30] Yang, Y., Yang, W., and Jiang, D., 2018, "Simulation and Experimental Analysis of Rolling Element Bearing Fault in Rotor-Bearing-Casing System," Eng Fail Anal, **92**, pp. 205–221.
[31] Yang, Y., Liu, C., Jiang, D., and Behdinan, K., 2020, "Nonlinear Vibration Signatures for Localized Fault of Rolling Element Bearing in Rotor-Bearing-Casing System," Int J Mech Sci, **173**.
[32] Xu, M., Song, Z., Ding, X., Li, G., Shao, Y., and Gu, J. X., 2022, "An Improved Dynamic Modelling for Exploring Ball Bearing Vibrations from Time-Varying Oil Film," Journal of Dynamics, Monitoring and Diagnostics, pp. 93–102.
[33] Kochi, T., Sakai, M., Nogi, T., Dong, D., and Kimura, Y., 2019, "Experimental Study on the Physics of Thick EHL Film Formation with Grease at Low Speeds," Tribol Lett, **67**(2).
[34] Cen, H., and Lugt, P. M., 2020, "Replenishment of the EHL Contacts in a Grease Lubricated Ball Bearing," Tribol Int, **146**.
[35] Zhang, X., and Glovnea, R., 2021, "Grease Film Thickness Measurement in Rolling Bearing Contacts," Proceedings of the Institution of Mechanical Engineers, Part J: Journal of Engineering Tribology, **235**(7), pp. 1430–1439.
[36] Martynenko, G., Chernobryvko, M., Avramov, K., Martynenko, V., Tonkonozhenko, A., Kozharin, V., and Klymenko, D., 2018, "Numerical Simulation of Missile Warhead Operation," Advances in Engineering Software, **123**, pp. 93–103.
[37] Vollan, A., and Komzsik, L., 2012, *Computational Techniques of Rotor Dynamics with the Finite Element Method*, CRC Press.
[38] Moes, H., 1992, *Optimum Similarity Analysis with Applications Lubrication*.
[39] Wu, W., Hong, J., Li, Y., and Li, X., 2017, "Investigation of Non-Uniform Preload Effect on Stiffness Behavior of Angular Contact Ball Bearings," Advances in Mechanical Engineering, **9**(3).
[40] Liu, J., Tang, C., Wu, H., Xu, Z., and Wang, L., 2019, "An Analytical Calculation Method of the Load Distribution and Stiffness of an Angular Contact Ball Bearing," Mech Mach Theory, **142**.
[41] Li, Z., Wang, C., Hu, X., Wang, H., and Yang, L., 2024, "Study on the Effect of Angular Misalignment and Axial Preload on the Mechanical Properties of Four-Point Angular Contact Ball Bearings," Mech Mach Theory, **193**, p. 105565.